Available online at www.sciencedirect.com
SCIENCE DIRECT®
International Journal of Heat and Mass Transfer 49 (2006) 1658–1666
International Journal of HEAT and MASS TRANSFER
www.elsevier.com/locate/ijhmt

Enhancement of thermal interface materials with carbon nanotube arrays

Jun Xu, Timothy S. Fisher *

School of Mechanical Engineering and Birck Nanotechnology Center, Purdue University, 1205 West State Street, West Lafayette, IN 47907-2057, United States

Received 18 January 2005; received in revised form 13 May 2005
Available online 6 January 2006

Abstract

This paper describes an experimental study of thermal contact conductance enhancement enabled by carbon nanotube (CNT) arrays synthesized directly on silicon wafers using plasma-enhanced chemical vapor deposition. Testing based on the one-dimensional reference bar method occurred in a high-vacuum environment with radiation shielding, and temperature measurements were made with an infrared camera. Results from other thermal interface materials are presented, as well as combinations of these materials with CNT arrays. Dry CNT arrays produce a minimum thermal interface resistance of 19.8 mm^2 K/W, while the combination of a CNT array and a phase change material produces a minimum resistance of 5.2 mm^2 K/W.
© 2005 Elsevier Ltd. All rights reserved.

Keywords: Carbon nanotube array; Thermal contact conductance enhancement; Thermal interface material

1. Introduction

Reduction of chip-package interfacial thermal resistance remains a major challenge in the thermal management of semiconductor devices. As projected in the International Technology Roadmap for Semiconductors (ITRS) 2004 Update [1], by 2018, power dissipation levels of "cost-performance" and "high-performance" single-chip devices will reach 1.08 and 0.64 W/mm^2, respectively. To achieve reliable packages for future devices, improved thermal interface materials will be required. Currently, some phase change materials (PCMs) produce low interfacial resistances [2]. However, in the application of most thermal interface materials including PCMs, high conductance is achieved primarily by enhancing the gap materials' spreadability and elasticity. Further, issues such as dry-out/pump-out and mechanical fatigue compromise the long-term reliability of many of these materials [3].

The high intrinsic thermal conductivity of carbon nanotubes [4–9] suggests many heat transfer enhancement applications. Choi et al. [10] measured the effective thermal conductivity of nanotube-in-oil suspensions and found that, with 1 vol% of nanotubes, the effective thermal conductivity increased significantly (more than twice the value of the base oil) though not nearly as much as a simple, above-threshold percolation model would predict [11]. Biercuk et al. [12] used single-walled nanotubes (SWNTs) to augment the thermal transport properties of industrial epoxy and found that epoxy loaded with 1 wt% unpurified SWNTs exhibited a 70% increase in thermal conductivity at 40 K and 125% at room temperature.

Recently, Xu and Fisher [13] have shown that the thermal contact resistance between silicon wafers and copper with a CNT array interface can be as low as 23 mm^2 K/W. They also have shown that CNT arrays with different properties produce measurable variations in thermal enhancement. In the present work, the CNT array height and coverage on samples was improved with a new catalyst configuration. In addition, the performance of other thermal interface materials (phase change material and indium

* Corresponding author. Tel.: +1 765 494 5627; fax: +1 765 494 0539.
E-mail address: tsfisher@purdue.edu (T.S. Fisher).

0017-9310/$ - see front matter © 2005 Elsevier Ltd. All rights reserved.
doi:10.1016/j.ijheatmasstransfer.2005.09.039

Nomenclature

A	area of the testing sample and reference bars (m^2)	*Greek symbols*	
L	distance between sections 1 and 2 (m)	Δ	difference
G	temperature gradient in the reference bars (K/m)	δ	uncertainty
k	thermal conductivity (W/mK)	ε	emissivity
P	pressure (Pa)	*Subscripts*	
q	heat flow in the test column (W)	1, 2	sections 1 and 2
R	thermal resistance (mm^2 K/W)	Cu	copper
R_a	average surface roughness (μm)	c	contact resistance
R_z	average peak-to-valley height of surface profile (μm)	i	upper or lower reference bar index
T	temperature (K)	L	lower reference bar
t	thickness of the test-sample (m)	Si	silicon
X	general variable used in uncertainty analysis	U	upper reference bar

sheet) and combinations of these materials with CNT arrays were also studied.

The following two sections of this paper describe the experimental setup for contact conductance measurements and the synthesis of carbon nanotube arrays. The subsequent section presents the measured results and discusses relevant observations. The final section concludes the work with a summary of the results and brief comments on areas for further study.

2. Experimental setup

In the present work, copper and single-crystal silicon have been selected as two representative interface substrate materials. The thermal contact resistances of the interface under different conditions were experimentally measured with a reference calorimeter setup (Fig. 1) based on axial one-dimensional steady-state heat conduction [14]. An electrical cartridge heater and a heat sink cooled by a chilled water loop maintained a constant heat flow q in the test column, which consists of two reference bars with the specimen located between. The reference bars with a uniform cross-section area A (10 mm × 10 mm) were made of oxygen-free high-conductivity copper (OFHC). The interface substrate was a 10 mm × 10 mm undoped, double-side-polished silicon chip with a thickness of $t = 270$ μm. An external force load also can be applied to the test column. Ball bearings ensured a parallel force vector to the axis of the column. A polished aluminum radiation shield (emissivity of 0.04) minimized radiation heat loss from the test column. The total heat loss from the test columns' radiating surfaces was estimated to be less than 1% of the input heat flow. The setup was situated in a vacuum chamber ($P \approx 1.33 \times 10^{-4}$ Pa) to prevent convective heat loss. Temperatures T_1 and T_2 were measured at sections 1 and 2 of Fig. 1, and L is the distance between the sections:

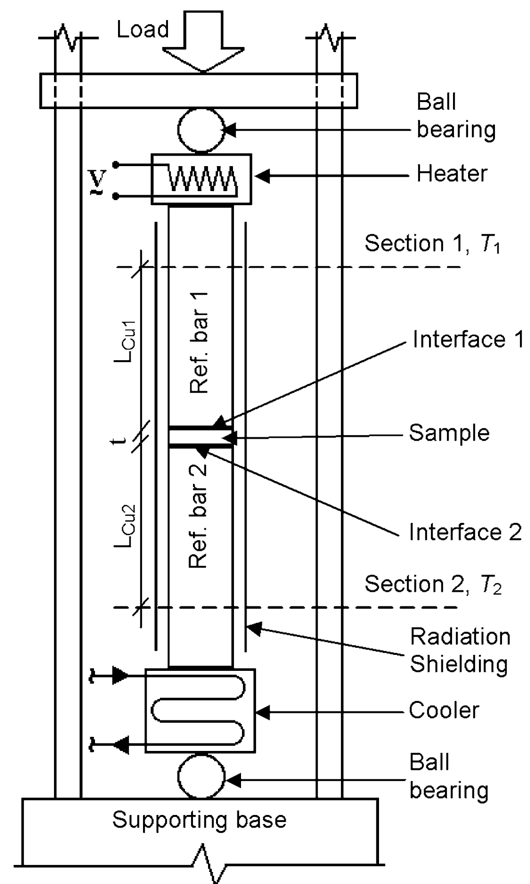

Fig. 1. Reference calorimeter experimental setup.

$$L = L_{Cu1} + t + L_{Cu2} \quad (1)$$

Surface roughness strongly influences thermal contact conductance [14]. In the present study, the surfaces of interface substrates were examined with a profilometer, and calculations of average roughness R_a and average

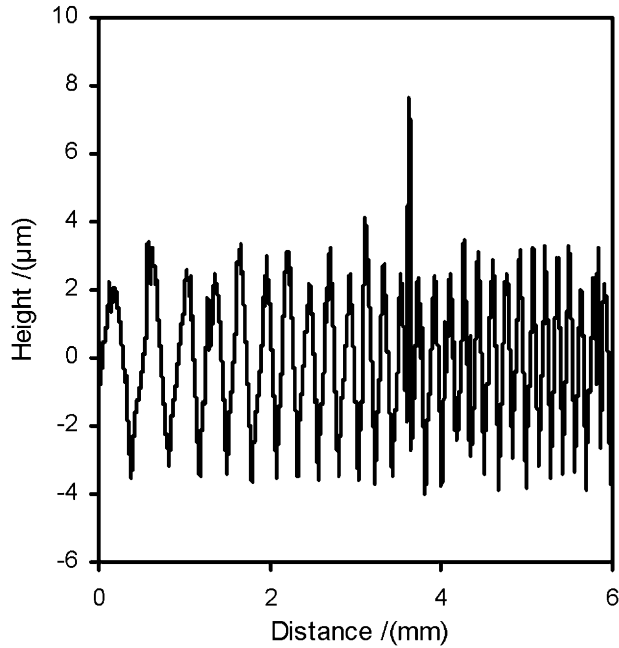

Fig. 2. A typical profilometer scan of the copper reference bar surface.

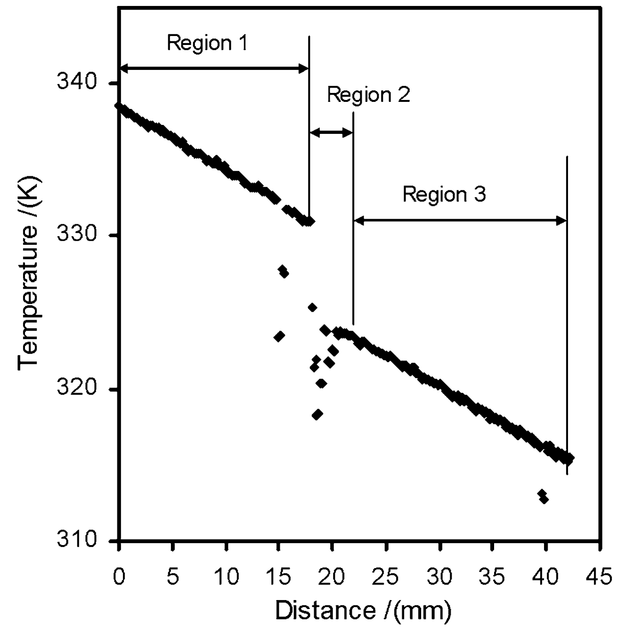

Fig. 3. A temperature profile of the test column measured with the thermal imaging system.

peak-to-valley height of the surface profile R_z [15, ASME B46.1-2002] were recorded to characterize the surface morphology. A typical surface morphological profile of the copper bar is illustrated in Fig. 2. The R_a and R_z values of this profile were 1.4 and 7.9 µm, respectively. The R_a and R_z values for the silicon wafer surface were 0.02 and 0.14 µm, respectively.

A three-dimensional heat conduction simulation of the experimental arrangement with radiation boundary conditions revealed that the difference between the vertical temperature gradients along the reference bars' surfaces and those along the central axis of the reference bars is less than 0.3%. Therefore, in the present study, instead of inserting the thermocouples into the reference bars, the surface temperature distributions of the bars were recorded by an infrared thermal imaging system (Flir SC300) and were used to quantify one-dimensional temperature distributions in the test column. To facilitate accurate temperature measurements, one lateral surface of each copper bar was painted with Rustoleum flat black paint to be grey and diffuse with high emissivity ($\varepsilon = 0.94$), and the vacuum system was equipped with a germanium viewport through which the thermal camera could view the apparatus. The temperature and distance measurements with the infrared system were carefully calibrated as reported previously [13].

Through imaging software, a virtual line parallel to the test column axis was drawn on the columns' exposed surfaces in the digital thermal image. Temperature readings for all pixels on this line were recorded simultaneously. The locations of sections 1 and 2 were chosen from the line, and then the corresponding temperatures (T_1 and T_2) and distance (L) were determined. Fig. 3 shows a typical temperature profile of the test column recorded by the thermal camera. Region 1 contains most of the upper reference bar; region 2 includes the interface specimen and portions of both reference bars near the interfaces; region 3 contains most of the lower bar. The discontinuous readings in Regions 1 and 3 correspond to the marks placed on the bar surfaces that were used for length calibration.

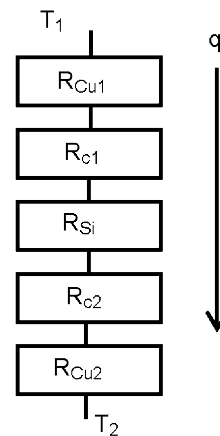

Fig. 4. Thermal circuit for the test column.

The thermal network for the test column is shown in Fig. 4. The total thermal resistance between the two sections is

$$R_{\text{total}} = R_{\text{Cu}} + R_{\text{c1}} + R_{\text{Si}} + R_{\text{c2}} \quad (2)$$

R_{Cu} represents the conductive thermal resistance of all the copper bars between the two sections

$$R_{\text{Cu}} = R_{\text{Cu1}} + R_{\text{Cu2}} = (L_{\text{Cu1}} + L_{\text{Cu2}})/(k_{\text{Cu}} \cdot A) \quad (3)$$

and R_{Si} is the conductive thermal resistance of the silicon wafer itself:

$$R_{Si} = t/(k_{Si} \cdot A) \tag{4}$$

R_{c1} and R_{c2} are the contact resistances for interfaces 1 and 2 (see Fig. 1), respectively. At steady state, the constant heat flow rate, q can be expressed as

$$q = -G \cdot k_{Cu} \cdot A \tag{5}$$

where G is the reference bar's temperature gradient, which was obtained by linear regression of temperature profiles recorded by the infrared camera. For the temperature profile shown in Fig. 3, the gradients in the upper and lower bars, G_U and G_L, respectively, differ by less than 3%. In the present experiments, the measured temperature gradients in the upper and lower copper bars always agreed to within 6%, and average values from the upper and lower bars were used for heat flow calculations.

With the temperature difference, $\Delta T = T_1 - T_2$, the value of R_{total} can be determined as

$$R_{total} = \Delta T/q \tag{6}$$

With known R_{total}, R_{Cu}, R_{Si} and R_{c2}, the measured interface resistance R_{c1} can be calculated from Eq. (2). In this work, the resistances at CNT–substrate interface, the CNT array's bulk resistance and any other thermal interface materials are grouped into the measured interface resistance.

In the present study, the uncertainty of the contact resistance measurements has been estimated using a standard error estimation approach [16]:

$$\delta R_{c1} = \left[\sum_{i=1}^{n}\left(\frac{\partial R_{c1}}{\partial X_i}\delta X_i\right)^2 + (\delta R_{c2})^2\right]^{1/2} \tag{7}$$

where $X_i = G_U$, G_L, ΔT, L, A, and k_{Cu}, δX_i is the uncertainty for each quantity X_i, and δR_{c2} is uncertainty in interface resistance from the control experiment. For the control experiments, R_{c1} is assumed to equal R_{c2}, and the second term on the right side of Eq. (7) is absent. In the present experiments, $\delta\Delta T$ was approximately ± 0.2 K with ΔT in the range of 20–30 K; δA was less than ± 0.004 cm^2; and δL was ± 0.18 mm with $L \approx 42$ mm based on pixel density and the reference marks discussed previously.

The temperature gradients G_i in the reference bars varied from 100 to 450 K/m for different experiments. The uncertainty in G_i was estimated by an established method for calculating 95% confidence intervals of slopes predicted by linear regression [17]. The resulting value of δG_i ranged from ± 2 to ± 3 K/m for a given reference bar.

Because of the small temperature variation in the experimental system, the thermal conductivities of OFHC copper and silicon in the calculations of resistances were assumed to take constant values of 390 W/(mK) [18] and 141 W/(mK) [19], respectively. The effects of δk_{Si} and δt were very small and neglected due to the small values of the t/L ratio and δt. However, the uncertainty in the copper bars' thermal conductivity $[\delta k_{Cu} = \pm 2\ \mathrm{W/(mK)}]$ was included in the analysis. The combined effects of δL, δA, and δk_{Cu} added an uncertainty of approximately ± 1 mm^2 K/W to δR_{c1}, and this value is generally much smaller than the effects of $\delta\Delta T$ and δG_i.

Further examination of Eqs. (5) and (6) reveals that the pre-factors (i.e., sensitivity coefficients) of $\delta\Delta T$ and δG_i in Eq. (7) are proportional to the inverse and the inverse square of the temperature gradient, respectively. Therefore, larger temperature gradients produce less uncertainty. For example, the uncertainty in contact resistance decreases from approximately ± 25 to ± 4 mm^2 K/W as G_i increases from 100 to 400 K/m. The estimated uncertainties for measured interface resistances are indicated by error bars in all subsequent graphical results.

Fig. 5 illustrates the test-section details for each experimental configuration considered in the present work. The

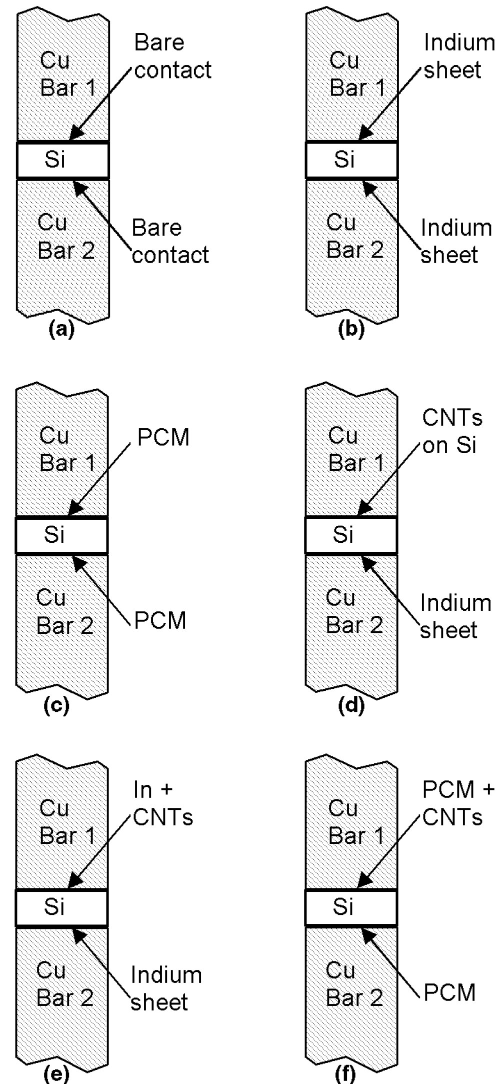

Fig. 5. Interface configurations for thermal contact resistance measurements of (a) Cu–Si, (b) Cu–In–Si, (c) Cu–PCM–Si, (d) Cu–CNT–Si, (e), Cu–In–CNT–Si, and (f) Cu–PCM–CNT–Si.

thermal contact resistances of copper–silicon (Cu–Si, Fig. 5(a)), copper–indium–silicon (Cu–In–Si, Fig. 5(b)), and copper–PCM–silicon (Cu–PCM–Si, Fig. 5(c)) were measured initially in control experiments. The thermal contact resistances of copper–CNT–silicon interfaces (Cu–CNT–Si, Fig. 5(d)) were then tested and compared to control results. Further, the indium sheet–CNT array and PCM–CNT array combinations (Fig. 5(e) and (f)) were tested to evaluate possible enhancement of interface conductance. Indium is a very soft, silvery-white metal whose melting point and thermal conductivity are 429.32 K and 82 W/(mK), respectively. The 370 μm-thick indium sheet tested in the present study was placed between copper and silicon surfaces. The phase change material tested was a 250 μm-thick pad (Honeywell PCM45F). Polymer-based PCM45F with a proprietary filler material exhibits a thermal conductivity of 3.0–5.0 W/(mK). In the present study, to ensure full adhesion, the pad was placed on the copper bar surface for more than one hour at room temperature, and then heat and pressure were applied to the pad to achieve a thickness of approximately 20 μm according to the manufacturer's specifications [20].

3. Fabrication of carbon nanotube arrays

All carbon nanotube array samples discussed in this work were grown on silicon wafers by direct synthesis with microwave plasma-enhanced chemical vapor deposition (PECVD) in which the feed gases are H_2 and CH_4. A wide range of parameters can be varied in PECVD processes to optimize the properties of the synthesized CNTs [21–23]. However, in the present study, the synthesis parameters were held constant to achieve samples with similar characteristics. The PECVD chamber's working pressure is 10 Torr, and the synthesis temperature was maintained at 800 °C with a microwave power of 150 W. The mass flow rates of H_2 and CH_4 were 72 and 8 sccm, respectively.

Fig. 6 shows a schematic of the substrate and structure produced by the PECVD carbon nanotube array synthesis process. The thicknesses of titanium, aluminum and nickel metal layers are 30, 10, and 6 nm, respectively. This configuration creates favorable surface conditions for CNT growth by PECVD on bare silicon wafers. The titanium layer promotes adhesion to the silicon wafer, and the aluminum layer has been shown to enhance CNT array growth with a nickel catalyst on silicon [24,25].

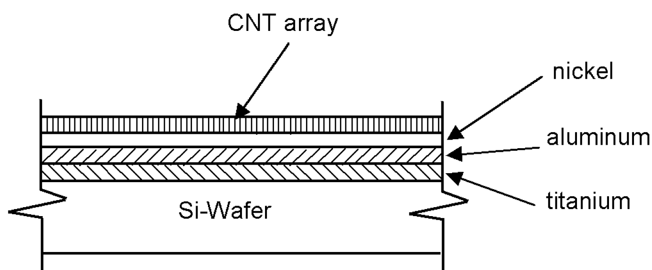

Fig. 6. Sketch of the CNT array and catalyst structure on a silicon wafer.

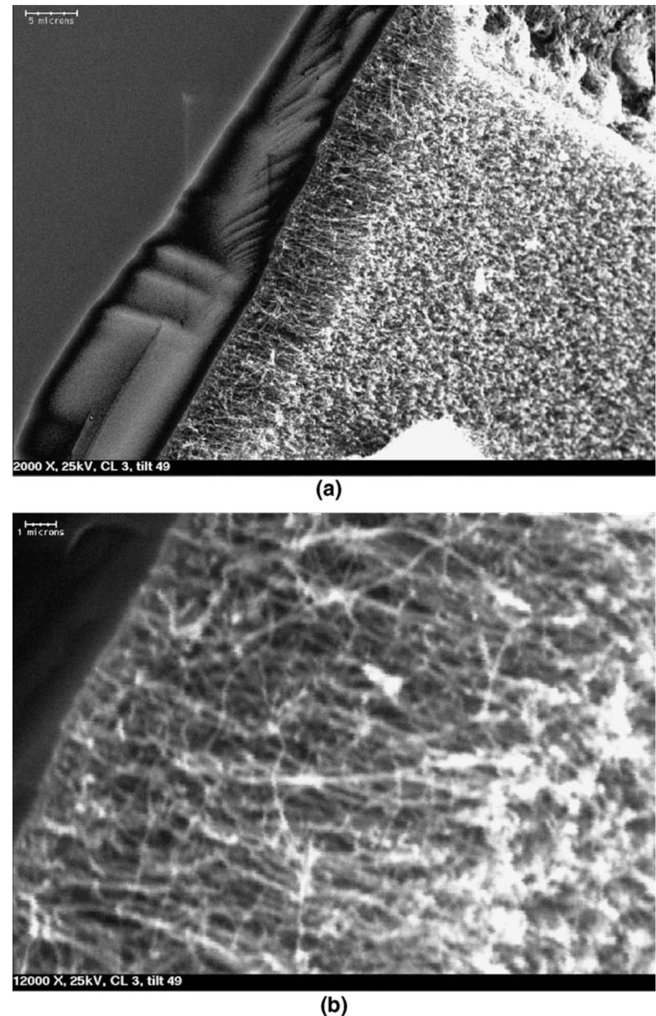

Fig. 7. SEM images of a CNT array viewed with a tilt angle of 49°: (a) typical appearance of the CNT array on a Si wafer (scale bar = 5 μm) and (b) high magnification view of a CNT array (scale bar = 1 μm).

The scanning electron microscope (JEOL-35CF) images in Fig. 7 reveal the typical structure of the CNT arrays. Fig. 7(a) shows that the array consists of dense and vertically oriented CNTs. The array also appears to possess a uniform layer thickness. At a higher magnification, the image in Fig. 7(b) shows the detailed structure of the array. The CNT array thickness was approximately 10 μm for all tested samples. Further, from the SEM images, the density of the array was estimated to be approximately 300 million CNTs per square millimeter. The growth substrate's mass was measured before and after synthesis with an analytical balance (Ainsworth M-220D), and the deposited carbon mass was estimated to be approximately 1.6 g/m^2 from these measurements.

The diameters and wall structure of the carbon nanotubes in the arrays were examined with a transmission electron microscope (JEOL 2000FX). The CNTs were extracted from an array by rubbing an ethanol-saturated

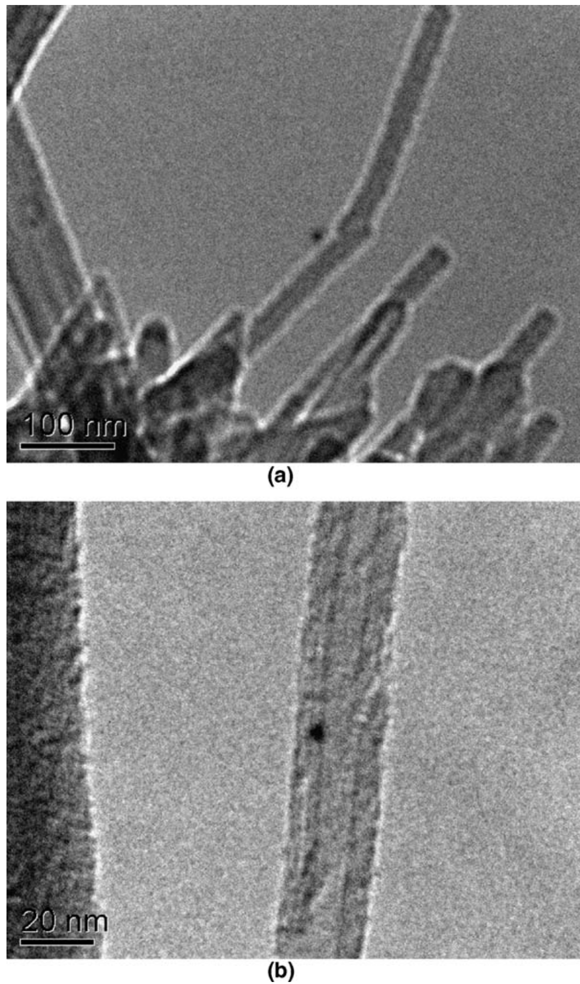

Fig. 8. TEM images of CNTs: (a) CNTs protruding from a bundle (scale bar = 100 nm) and (b) high magnification view of a multi-walled CNT showing wall structure (scale bar = 20 nm).

TEM grid over the array. Fig. 8(a) shows several straight CNTs protruding from a bundle and having very similar diameters. Fig. 8(b) clearly shows that the individual structure is a multi-walled nanotube with an outer diameter of approximately 20 nm.

4. Results and discussion

Fig. 9 shows the measured resistances for the Cu–Si and Cu–CNT–Si configurations. A previous result [13] from a sample with a 7 μm array height is also included in the figure. The resistance measurements of the present Cu–CNT–Si interface with a 10 μm CNT array height exhibit less pressure dependence and much smaller contact resistances than the previous result. For the present CNT array sample, all measured resistances under the tested loads are less than 31 mm^2 K/W, and the lowest value is 19.8 mm^2 K/W at a pressure of 0.445 MPa.

We postulate that the larger CNT array height improves substrate-to-substrate contact across the microscopic gaps that are caused primarily by the roughness of the copper

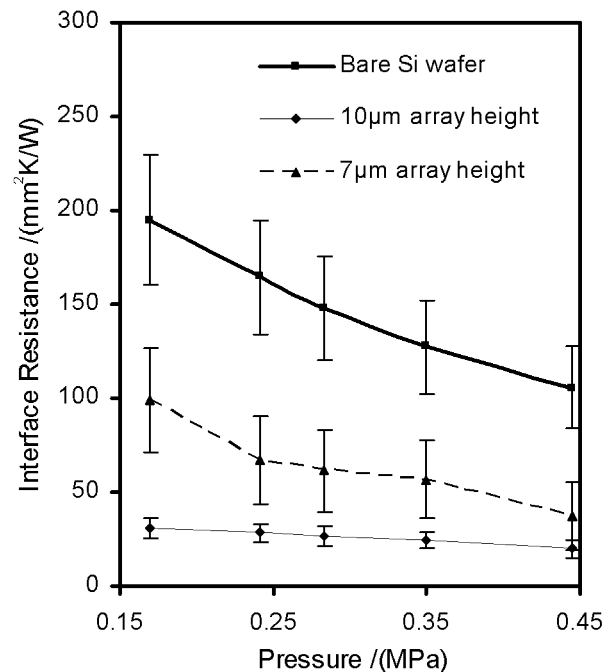

Fig. 9. Thermal resistance as a function of pressure for Cu–Si and Cu–CNT–Si interfaces.

surface. The average peak-to-valley height R_z for the profile depicted in Fig. 2 is 7.9 μm, which is larger than the previous CNT array height of 7 μm. Conversely, the present CNT array height of 10 μm is larger than R_z and would allow the CNT matrix to bridge most, if not all, interfacial gaps at all applied pressures. This hypothesis based on gap bridging is also supported by the smaller pressure dependence of thermal resistance for 10 μm array. Contact resistance for this taller array decreases by approximately 35% as pressure increases from 0.169 to 0.445 MPa; while for the shorter array, the decrease in resistance is approximately 60% over the same pressure range. Given that the short array's CNT height was only slightly smaller than the peak-to-valley roughness parameter R_z, increasing mechanical deformation may have allowed new CNT clusters to bridge interfacial gaps as pressure increased, thus producing larger pressure dependence.

The SEM image in Fig. 10 illustrates the post-experiment surface topography of a CNT array on a silicon substrate. The image clearly demonstrates that the dense and flexible CNT array's top surface was compressed and conformed well to the surface profile of the copper bar. The image also indicates that the CNT arrays were well anchored to the substrates without being removed after undergoing the experiments.

Experiments on the indium sheet alone and in combination with a CNT array revealed moderate interface resistance and pressure dependence, as shown in Fig. 11. The measured resistance of the Cu–In–Si interface ranges from 27.2 to 18.5 mm^2 K/W. These resistances are much lower than those from the bare Cu–Si case (see Fig. 10); however, they are higher than the reported contact resistance with

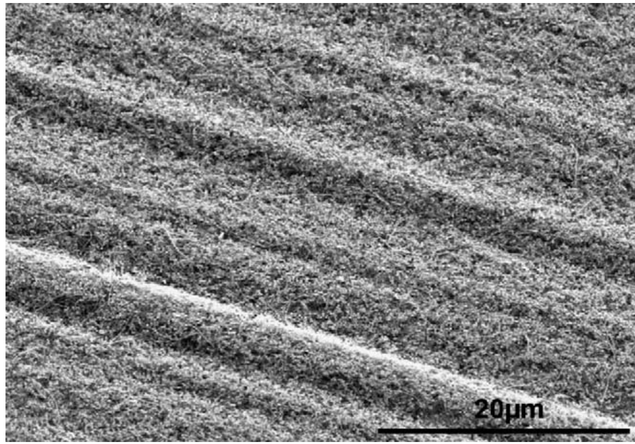

Fig. 10. SEM image of a post-experiment CNT array on silicon.

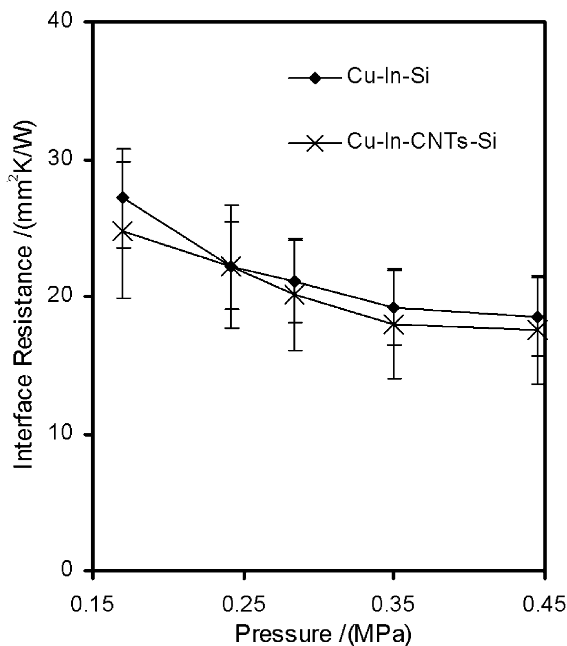

Fig. 11. Thermal resistance as a function of pressure for copper–silicon interfaces with an indium sheet (Cu–In–Si) and an indium sheet in combination with a CNT array (Cu–In–CNT–Si).

reflowed solder [3]. Even though indium is very soft and can be made to cold-flow between two non-uniform surfaces, cold-flow requires high pressures that cause the surface layer of indium to become more shear-resistant and therefore to stick to the surface. Consequently, the mobility of indium at the interface is much less than that for reflowed solder, and the bonding between the indium sheet and contacted surface is also much weaker than that of a soldered interface. Results for the Cu–In–CNT–Si configuration indicate that the addition of the CNT array may reduce interface resistance slightly for most pressures, but all comparative differences lie within the error bars. The similarity in thermal performance suggests that the thick (370 μm) indium sheet under moderate pressures conforms reasonably well to the surfaces and therefore likely bridges gaps in a manner that is similar to the CNTs alone. The CNTs in combination with the indium sheet do not enhance interfacial heat transfer because they likely do not penetrate the indium to form a true composite material, but instead form a compressed layer beneath the indium to create two, local series resistances—one through the compressed CNT layer and the other through the indium.

The thermal interface resistance of phase change materials can exhibit strong temperature dependence because of the material's changing viscosity. To avoid outgassing in the high vacuum environment, experiments were conducted at a relatively low heat flow with a nominal interface temperature of 313 K, and results are shown in Fig. 12. The measured resistances of the Cu–PCM–Si interface range from 52.2 to 16.2 mm^2 K/W. At the same interface temperature, the addition of CNTs (Cu–PCM–CNT–Si) significantly reduces the resistance. For the Cu–PCM–CNT–Si interface, the lowest measured resistance value is 5.2 mm^2 K/W at a pressure of 0.35 MPa. The PCM–CNT array composite may have a much higher effective thermal conductivity compared to the PCM itself, and therefore the contact conductance improves. The two configurations show similar pressure-resistance characteristics, with lower resistances for increasing load. The resistances decrease dramatically between the pressures of 0.24 and 0.28 MPa, and then become more stable at higher pressure. This pressure dependence can be attributed to the preparation of the tested interfaces. As mentioned above, the PCM layers were pre-formed under a

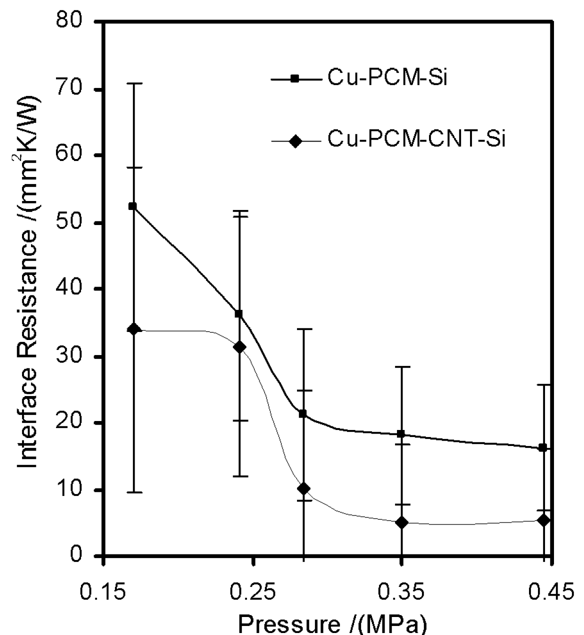

Fig. 12. Thermal resistance as a function of pressure for copper–silicon interfaces with the addition of PCM (Cu–PCM–Si) and in combination with a CNT array (Cu–PCM–CNT–Si).

temperature higher than the PCM melting point at a pressure of 0.28 MPa, and the effective thicknesses were approximately 20 μm. With a pressure less than 0.28 MPa and a temperature of 313 K, the very thin PCM layer apparently does not act as an effective adhesive and is not able to fill all the gaps. Nevertheless, as the pressure increases above 0.28 MPa, the thin PCM layer is capable of filling all the microscopic voids. It was also observed that the PCM did not wet the CNT array well under the low pressure. Increased pressure helps the CNT array to penetrate the PCM, and the resulting resistance decreased significantly. Fig. 12 also indicates that, with a resistance less than $10\ mm^2\ K/W$, the measurement uncertainty of the present experimental setup is similar in magnitude to the measured resistance value.

5. Summary and conclusions

In this work, new CNT arrays with a tri-layer catalyst configuration have been fabricated by direct PECVD synthesis as heat-conduction interfaces. A reference calorimeter testing rig in a high-vacuum environment with infrared thermography has been used to measure the thermal contact characteristics. Thermal contact resistances between copper and an undoped silicon wafer were measured with carbon nanotubes, a phase change material, and indium sheet as interface layers. The CNT array's performance is comparable to that of indium sheet and phase change material, with a minimum resistance of $19.8\ mm^2\ K/W$ at a pressure of 0.445 MPa. Combinations of CNTs with both indium sheet and PCM were also evaluated. Compared to the Cu–In–Si interface, the addition of the CNT array slightly reduced the resistance. The addition of the CNT array greatly reduced the PCM–CNT array composite's thermal interface resistance. Under a load of 0.35 MPa, the PCM–CNT array combination produces a minimum thermal interface resistance of $5.2\ mm^2\ K/W$.

In general, the present study shows that free-standing CNT arrays can be very good thermal interface materials under moderate load compared to indium sheet and phase-change thermal interface materials. Further, combinations of CNT arrays and existing thermal interface materials can improve these materials' thermal contact conductance. In this work, all CNT arrays were synthesized under identical conditions. Variation of CNT array parameters including array density, diameter, and alignment, deserves further study to explore their effects on enhancement of thermal contact conductance. To undertake the measurement of resistances less than $5\ mm^2\ K/W$, the current experimental method should be revised to improve the measurement accuracy.

Acknowledgements

The authors gratefully acknowledge funding from the Cooling Technologies Research Center at Purdue University in support of this work and the thermal interface materials supplied by Honeywell Electronic Materials.

References

[1] International Technology Roadmap for Semiconductors, 2004 Update, jointly sponsored by the European Semiconductor Industry Association, Japan Electronics and Information Technology Industries Association, Korea Semiconductor Industry Association, Taiwan Semiconductor Industry Association, and the Semiconductor Industry Association, 2004.
[2] D.D.L. Chung, Thermal interface materials, J. Mater. Eng. Perform. 10 (2001) 56–59.
[3] D. Blazei, Thermal interface materials, Electron. Cool. 9 (4) (2003) 14–20.
[4] S. Berber, Y.K. Kwon, D. Tomanek, Unusually high thermal conductivity of carbon nanotubes, Phys. Rev. Lett. 84 (20) (2000) 4613–4617.
[5] J.W. Che, T. Cagin, W.A. Goddard, Thermal conductivity of carbon nanotubes, Nanotechnology 11 (2) (2000) 65–69.
[6] P. Kim, L. Shi, A. Majumdar, P.L. McEuen, Thermal transport measurements of individual multiwalled nanotubes, Phys. Rev. Lett. 87 (2001) 215502-1–215502-4.
[7] S. Maruyama, A molecular dynamics simulation of heat conduction of a finite length single-walled carbon nanotube, Microscale Thermophys. Eng. 7 (2003) 41–50.
[8] S. Lepri, R. Livi, A. Politi, Thermal conduction in classical low-dimensional lattices, Phys. Rep. 377 (1) (2003) 1–80.
[9] C. Yu, W. Jang, D. Kim, Z. Yao, L. Shi, D. Li, A. Majumdar, Thermal and thermoelectric measurements of low dimensional nanostructures, in: Proceedings of the 2003 ASME Summer Heat Transfer Conference, HT2003-47263, 2003, pp. 1–6.
[10] S.U.S. Choi, Z.G. Zhang, W. Yu, F.E. Lockwood, E.A. Grulke, Anomalous thermal conductivity enhancement in nanotube suspensions, Appl. Phys. Lett. 79 (14) (2001) 2252–2254.
[11] S.T. Huxtable, D.G. Cahill, S. Shenogin, L. Xue, R. Ozisik, P. Barone, M. Usrey, M.S. Strano, G. Siddons, M. Shim, P. Keblinski, Interfacial heat flux in carbon nanotube suspensions, Nature Mater. 2 (2003) 731–734.
[12] M.J. Biercuk, M.C. Llaguno, M. Radosavljevic, J.K. Hyun, A.T. Johnson, J.E. Fischer, Carbon nanotube composites for thermal management, Appl. Phys. Lett. 80 (15) (2002) 2767–2769.
[13] J. Xu, T.S. Fisher, Enhanced thermal contact conductance using carbon nanotube arrays, in: ITherm 2004 Proceedings: Ninth Intersociety Conference on Thermal and Thermomechanical Phenomena in Electronic Systems, Las Vegas, NV, 2004. pp. 549–555.
[14] C.V. Madhusudana, Thermal Contact Conductance, Springer-Verlag, New York, 1996, pp. 23–67.
[15] Surface Texture, Surface Roughness, Waviness and Lay: ASME B46.1-2002, American Society of Mechanical Engineers, 2003.
[16] J.P. Holman, Experimental Methods for Engineers, sixth ed., McGraw Hill, New York, 1994, pp. 49–62.
[17] A.L. Bowker, G.J. Lieberman, Engineering Statistics, second ed., Prentice-Hall, Englewood Cliffs, NJ, 1972, pp. 325–364.
[18] Technical Data Sheet Copper 102, Rev. 1, Hamilton Precision Metals, Inc., Lancaster, PA, 2001.
[19] S.P. Bates, Silicon Wafer Processing, Industry Initiatives for Science and Math Education (IISME), San Jose, CA, 2000.
[20] PCM45 Series Phase Change Thermal Interface Materials, Product Bulletin-Interconnect Packaging Solutions, PB0520703, Rev. 5, Honeywell Electronic Materials, Sunnyvale, CA, 2003.
[21] T. Hirata, N. Satake, G.H. Jeong, T. Kato, R. Hatakeyama, K. Motomiya, K. Tohji, Magnetron-type radio-frequency plasma control yielding vertically well-aligned carbon nanotube growth, Appl. Phys. Lett. 83 (6) (2003) 1119–1121.

[22] Y. Shiratori, H. Hiraoka, Y. Takeuchi, S. Itoh, M. Yamamoto, One-step formation of aligned carbon nanotube field emitters at 400 K, Appl. Phys. Lett. 82 (15) (2003) 2485–2487.
[23] T. Kato, G.H. Jeong, T. Hirata, R. Hatakeyma, K. Tohji, K. Motomiya, Single-walled carbon nanotubes produced by plasma-enhanced chemical vapor deposition, Chem. Phys. Lett. 381 (2003) 422–426.
[24] L. You, W.T. Chang, M. Tabib-Azar, Selective growth of carbon nanotubes by catalyst poisoning, in: Annual APS March Meeting 2004, Montreal, Que., Canada, 2004.
[25] A.M. Cassell, N.R. Franklin, T.W. Tombler, E.M. Chan, J. Han, H. Dai, Directed growth of free-standing single-walled carbon nanotubes, J. Am. Chem. Soc. 121 (1999) 7975–7976.